

Gaussian resource based heralded entangled state generation enhanced by photon addition and subtraction

Yun-Long Cao,^{1,2,3,4} Xiao-Ye Xu,^{1,2,3,4,*} Chuan-Feng Li,^{1,2,3,4,†} and Guang-Can Guo^{1,2,3,4}

¹*Laboratory of Quantum Information, University of Science and Technology of China, Hefei 230026, China*

²*Anhui Province Key Laboratory of Quantum Network,*

University of Science and Technology of China, Hefei 230026, China

³*CAS Center for Excellence in Quantum Information and Quantum Physics,*

University of Science and Technology of China, Hefei 230026, China

⁴*Hefei National Laboratory, University of Science and Technology of China, Hefei 230088, China*

(Dated: March 2, 2026)

We propose a heralded entanglement generation scheme based on Gaussian sources augmented with photon addition and subtraction operations. By combining single-mode squeezing, linear interferometers, and conditional photon-number measurements on ancillary modes, our model probabilistically generates dual-rail encoded Bell, GHZ, and W states. We systematically optimize the squeezing parameters and interferometer settings to maximize both the heralding success probability and the fidelity with the target states. Our results show that the inclusion of photon addition and subtraction significantly enhances the non-classicality of the output states, leading to improved generation performance, while maintaining computational efficiency comparable to single-photon source models. We further analyze the robustness of the scheme under parameter perturbations, demonstrating stable performance against realistic experimental imperfections. This work provides a versatile and experimentally feasible framework for scalable heralded entanglement generation using Gaussian resources with non-Gaussian operations.

I. INTRODUCTION

Quantum entanglement, a hallmark distinction between quantum and classical systems, is widely recognized as a foundational resource for quantum information technologies [1–3] and has been deeply exploited for tasks such as quantum key distribution, quantum teleportation, one-way quantum computing, quantum metrology, and so on [4–7]. The rapid advancement of quantum applications and the ongoing pursuit of quantum supremacy are driving the demand for large-scale quantum resources, thereby motivating the development of entangled states in both high-dimensional and many-body regimes [8–10]. Consequently, the efficient generation of such states has emerged as a pivotal challenge in advancing quantum technologies.

As for the photonic quantum information, Gaussian states or Gaussian operations constitute a category of great concern [11, 12]. They are relatively easy to prepare and highly stable for scaling up the experimental system. However, Gaussian states and operations are fundamentally limited, as they cannot directly produce some non-classical states or maximally entangled states which can be useful for showing quantum advantage [13–15]. To overcome this restriction, the non-Gaussian operation like conditional measurements, photon addition and subtraction are introduced to enable the probabilistic generation via post-selection and heralding [16–20]. This method inevitably suffers from rapidly decreasing success

probabilities and increasing system complexity when the scale of entanglement expands. Optimizing both the success rate and the quality of entanglement is therefore of crucial importance for realizing quantum applications on optical platforms.

Recent studies have explored several approaches to probabilistic entanglement generation. There are some works relying on single-photon sources based on quantum dots or on heralded parametric down-conversion processes [21–25]. Using Gaussian states merely to probabilistically preparing photonic entangled state is another line of work [16, 26], while subsequent work incorporates additional single photons to improve the efficiency of state preparation [27]. Using non-Fock basis to encode entangled states like cat-basis [28, 29] or inputting heralded states from Gaussian sources [30] are feasible directions for efficient generation of entanglement. These approaches can be efficiently integrated with emerging experimental platforms such as large-scale photonic integrated circuits [31, 32] and Gaussian boson sampling [33], thereby offering new models and promising directions for future quantum technologies.

In this work, we employ Gaussian states and photon-number detection as resources to extend heralded state generation toward entangled states, including Bell states, GHZ states, and W states, encoded on Fock basis. This work integrates the approaches of continuous-variable and discrete-variable schemes in the field of heralded entanglement generation, thereby extending the applicability and potential applications of this method across different physical platforms. By introducing heralded photon addition and subtraction, we further enhance the non-Gaussianity of the system, aiming to achieve superior performance in entanglement generation.

* xuxiaoye@ustc.edu.cn

† cffi@ustc.edu.cn

II. BACKGROUND

For a composite system defined in the Hilbert space H , that is a direct product of the relevant subsystem spaces $H = \otimes_{l=1}^n H_l$, the total state of the system in the form

$$|\psi\rangle = \sum_{i_1, \dots, i_n} c_{i_1, \dots, i_n} |i_1\rangle \otimes |i_2\rangle \otimes \dots \otimes |i_n\rangle \quad (1)$$

is separable when it can be described as a product of states in the subsystem spaces $|\psi\rangle = |\psi_1\rangle \otimes |\psi_2\rangle \otimes \dots \otimes |\psi_n\rangle$, and the states that are not separable are called entangled. In the bipartite system with both 2-dimension subspaces there are the maximally entangled states called Bell states,

$$\begin{aligned} |\psi^\pm\rangle &= \frac{1}{\sqrt{2}}(|0\rangle|1\rangle \pm |1\rangle|0\rangle), \\ |\phi^\pm\rangle &= \frac{1}{\sqrt{2}}(|0\rangle|0\rangle \pm |1\rangle|1\rangle), \end{aligned} \quad (2)$$

which are well known for the nonlocal inequality test [34]. In multipartite systems, the structure of entanglement becomes significantly more intricate, and there may exist inequivalent forms, considering three qubits for instance, we have two inequal maximal entangled states, Greenberger–Horne–Zeilinger (GHZ) $|\text{GHZ}\rangle = \frac{1}{\sqrt{2}}(|000\rangle + |111\rangle)$ and W $|\text{W}\rangle = \frac{1}{\sqrt{3}}(|001\rangle + |010\rangle + |100\rangle)$ states. These states cannot be generated from the separable states by local operations and classical communication (LOCC), making their efficient generation a core challenge.

The problems involving multi-mode Gaussian states are typically formulated within continuous-variable (CV) quantum systems, where information is encoded in the quadratures of bosonic modes rather than in discrete two-level systems [11]. An N -mode bosonic system can be described by the quadrature operators of each mode defined in terms of creation and annihilation operators as

$$\hat{q}_i = (\hat{a}_i + \hat{a}_i^\dagger)/\sqrt{2\hbar}, \quad \hat{p}_i = -i(\hat{a}_i - \hat{a}_i^\dagger)/\sqrt{2\hbar}. \quad (3)$$

We define an operator vector $\mathbf{x} = (q_1, p_1, \dots, q_N, p_N)$. The Gaussian states can be completely characterized by the first and second moments of the operator vector. The first moment is called the displacement vector $\bar{\mathbf{x}} = \langle \hat{\mathbf{x}} \rangle$ and the second moment is called the covariance matrix \mathbf{V} with elements $V_{ij} = \frac{1}{2}(\langle \hat{x}_i \hat{x}_j + \hat{x}_j \hat{x}_i \rangle - \langle \hat{x}_i \rangle \langle \hat{x}_j \rangle)$. The Wigner function providing a quasi-probability representation of quantum states in phase space can completely characterize the CV quantum states. Gaussian states are named for the Wigner functions take the form of Gaussian distributions as

$$W_G(\mathbf{x}) = \frac{\exp[-\frac{1}{2}(\mathbf{x} - \bar{\mathbf{x}})^T \mathbf{V}^{-1}(\mathbf{x} - \bar{\mathbf{x}})]}{(2\pi)^N \sqrt{\det \mathbf{V}}}. \quad (4)$$

The Gaussian operation transforms Gaussian states into Gaussian states. The unitary Gaussian operation

generated from the Hamiltonian which is second-order polynomial of the mode operators can be described by a symplectic transformation S and a displacement d in terms of the quadrature operators. The operator vector and the covariance matrix transform as

$$\bar{\mathbf{x}} \rightarrow S\bar{\mathbf{x}} + d, \quad \mathbf{V} \rightarrow S\mathbf{V}S^T. \quad (5)$$

Gaussian operations including displacements, squeezing and linear mode transformation are naturally realized by optical devices, which offers a practical advantage for experimental realization. Partial tracing is a nonunitary Gaussian operation since tracing over modes corresponds mathematically to removing the degrees of freedom in phase space. The reduced state is a Gaussian state characterized by the displacement vector and the covariance matrix removing the excluded modes. This property ensures that the description remains within the Gaussian formalism even for conditional states of subsystems [35].

Performing local photon-number measurements from a multi-mode Gaussian state yields the probability distribution on the Fock basis [33, 36]. For a state characterized by the covariance matrix \mathbf{V} and a zero displacement vector, the probability of a specific measurement outcome $\hat{\mathbf{n}} = \otimes_j^M |n_j\rangle \langle n_j|$ is

$$P(n) = \frac{\text{Haf}(A_S)}{\mathbf{n}! \sqrt{|\mathbf{V}_Q|}}, \quad (6)$$

where

$$\mathbf{V}_Q = \mathbf{V} + I_{2M}/2, \quad (7)$$

$$A = \begin{bmatrix} 0 & I_{2M} \\ I_{2M} & 0 \end{bmatrix} (I_{2M} - \mathbf{V}_Q^{-1}), \quad (8)$$

and A_S is a submatrix from A that the rows and columns S remain depending on the measurement outcome. The Hafnian is a matrix function summing over all perfect matching permutations. Coherent contributions are present in the distribution when the displacement vector is non-zero. The probability is

$$\begin{aligned} P(n) &= \frac{\exp(-\frac{1}{2}\mathbf{x}^\dagger \mathbf{V}_Q^{-1} \mathbf{x})}{\mathbf{n}! \sqrt{|\mathbf{V}_Q|}} (\text{Haf}(A_S) + \\ &\sum_{j_1, j_2, j_1 \neq j_2} F_{j_1} F_{j_2} \text{Haf}(A_{S-\{j_1, j_2\}}) + \\ &\dots + \prod_j^{2M} F_j), \end{aligned} \quad (9)$$

where $\mathbf{F} = \mathbf{x}^\dagger \mathbf{V}_Q^{-1}$. Because of the computational complexity of Hafnian in the #P class, Gaussian boson sampling has emerged as a leading platform for demonstrating quantum computational advantage.

Post-selection is a probabilistic strategy that achieves desired results by conditioning on specific measurement

outcomes while discarding others. For instance, photon pair generated in spontaneous parametric down-conversion (SPDC) sources are probabilistic. If and only if coincidence counting happens at the detectors, the entangled states or single photons are extracted from all of states. Heralding is a conditional method with the measurements on ancillary modes. The detection of a specific outcome signals the presence of the desired results in other modes which enable the heralded states to serve as deterministic resources in next steps, such as heralded single photons from SPDC and single-mode nonlinear operations. For a pure state, when a measurement outcome \mathbf{h} is obtained on the ancillary modes with probability p , the total state can be decomposed into the following form,

$$|\psi\rangle = \sqrt{p}|\phi\rangle|\mathbf{h}\rangle + \sqrt{1-p}|R\rangle \quad (10)$$

while $|\phi\rangle$ is the output state and $|R\rangle$ is the rest state discarded by heralding [21]. Both the success probability and the quality of the target state are required for the entanglement generation.

III. METHOD

A heralded Gaussian model can be divided into two essential steps: the preparation of Gaussian states and the measurement on ancillary modes. Experimentally multi-mode Gaussian states are typically generated from multiple single-mode squeezed vacuum states with linear mode transformations decomposed into a finite network of two-mode transformations, while the heralding state is one of the Fock bases on the ancillary modes separated locally from the output modes. When a specific set of photon numbers are detected on the ancillary modes, the output modes are projected into a conditional state that coincides well with the target entangled state as a successful heralded generation.

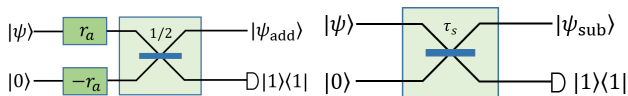


FIG. 1. Schematic of photon subtraction using a beam splitter and photon addition using single-mode squeezing. The squeezing parameter r_a for photon addition and the beam splitter transmissivity τ_s for photon subtraction are set to 0.8 and 0.1 in our model.

Moreover, additional modes and Gaussian operations can be introduced to achieve photon addition and subtraction enhancing the non-Gaussianity and non-linearity. A parametric amplifier or a beam splitter combined with a photon-number detector enable the probabilistic photon addition or subtraction operation in the optical system, which can be incorporated into the heralded Gaussian model with more modes. Owing

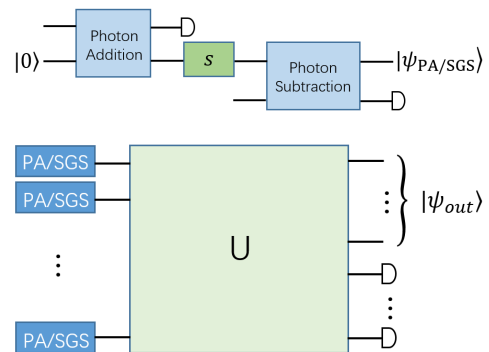


FIG. 2. Schematic of heralded entanglement generation model with photon addition/subtraction Gaussian source. The single-mode squeezers S and the linear interferometer U are serving as optimization parameters.

to the similar action of both single photons and Gaussian states with linear mode transformations, our model places photon-addition and subtraction operations adjacent to squeezing operations for obvious impact.

The target state is encoded by dual-rail encoding method that each qubit is represented by occupation in distinct local modes. For the Bell, GHZ and W state, the physical states are

$$|\text{Bell}\rangle = \frac{1}{\sqrt{2}}(|1010\rangle + |0101\rangle), \quad (11)$$

$$|\text{GHZ}\rangle = \frac{1}{\sqrt{2}}(|101010\rangle + |010101\rangle), \quad (12)$$

$$|\text{W}\rangle = \frac{1}{\sqrt{3}}(|101001\rangle + |100110\rangle + |011010\rangle), \quad (13)$$

described with the multi-mode Fock basis. Each basis component of the superposition state is encoded in at least one independent mode, so that the relative phases of the superposition can be directly controlled through single-mode phase rotations, overcoming the limitation that local photon-number measurements cannot reveal phase information. The quality of the heralded entangled state generation is assessed by both the heralded success probability and the fidelity with the target state. To achieve optimal performance in experiments, we optimize the parameters of single-mode squeezing and the linear interferometer under fixed conditions of photon addition/subtraction and heralding states.

The cost function is

$$f(\boldsymbol{\xi}) = -w_1 \ln(p) - w_2 \ln(F) + \epsilon \sum \|\xi_i\|^2, \quad (14)$$

where the success probability p and the fidelity $F = |\langle \psi_{output} | \psi_{target} \rangle|^2$ are defined by the probabilities of Fock basis measurement. The numerical computation in CV quantum system is performed with support on The Walrus package [37]. There is a challenge of evaluating conditional probabilities in single-photon models that summing over all possible measurement outcomes corre-

sponding to successful heralding is difficult, but the closure of Gaussian states under partial trace confines the computational complexity to that of computing a Hafnian of the reduced state.

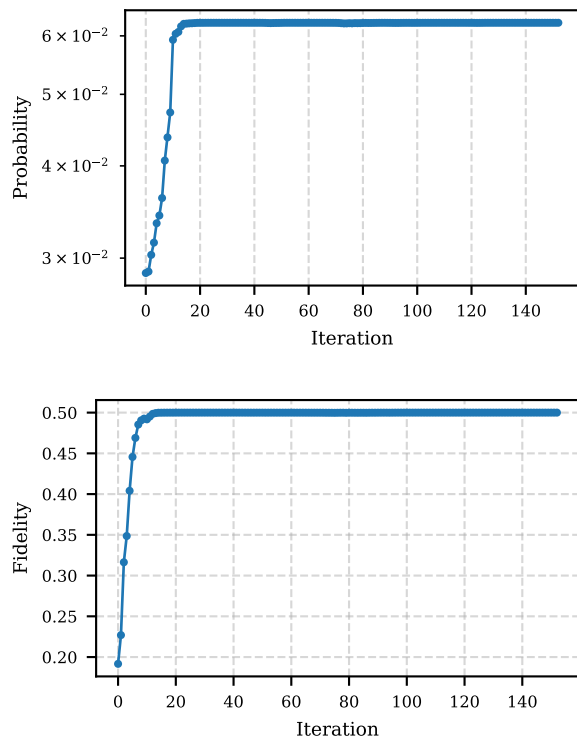


FIG. 3. Probability and fidelity of the Bell state generated as a function of optimal steps. The weights w_1 , w_2 and ϵ are set to 10, 1 and 10^{-4} .

The schematic of the proposed heralded entanglement generation model is illustrated in Fig. 1 and 2. The Gaussian source is composed of a basic single-mode squeezed state combined with heralded photon addition and subtraction. Photon addition is realized by preparing a two-mode squeezing state, which can be equivalently implemented using two single-mode squeezers followed by a balanced beam splitter. When a single photon is detected on the ancillary mode, the other mode is conditionally projected onto a state with one additional photon. Similarly, photon subtraction is realized by interfering the modes with vacuum on a beam splitter and detecting a single photon on the ancillary mode, thereby heralding photon subtraction on the other mode. Photon addition is applied before the single-mode squeezing to exploit possible stimulated effects, while photon subtraction is performed after the squeezing to mitigate vacuum-induced errors.

The linear optical interferometer is constructed by cascading multiple beam splitters and phase shifters, enabling the decomposition of any multimode interferometer $SU(n)$ into a sequence of $SU(2)$ transformations [38]. Heralding measurements are implemented via

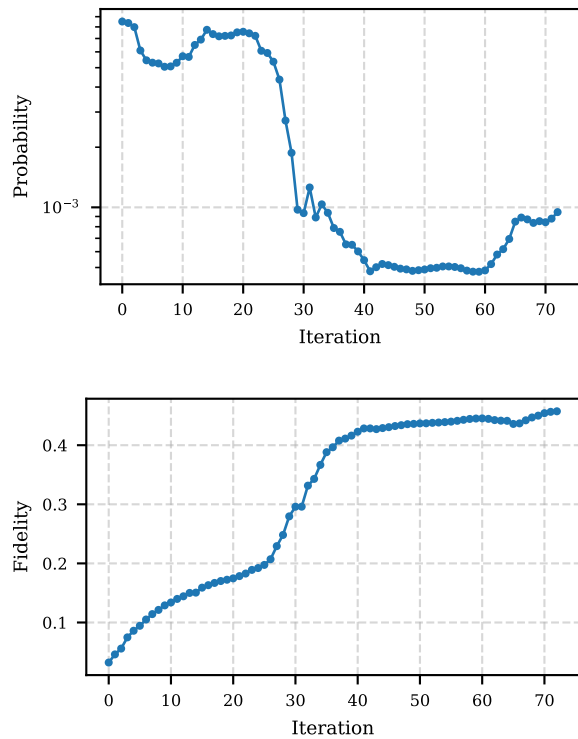


FIG. 4. Probability and fidelity of the GHZ state generated as a function of optimal steps. The weights w_1 , w_2 and ϵ are set to 10, 1 and 10^{-4} .

single-mode photon-number-resolving detections, which project the Gaussian state onto the multimode Fock basis. In this framework, the heralding modes conditionally project the output modes onto entangled states—such as Bell or GHZ states—depending on the parameters and measurement outcomes. Since the vacuum component inherent in Gaussian states limits the nonclassicality of the heralded states, post-selection on the output modes can be employed to exclude vacuum events.

IV. RESULTS

A. Optimization Procedure

The rapid and stable convergence of the probability and fidelity during optimization process is the basis for application and expansion. We can plot the probability and fidelity of the entangled state as functions of optimization steps at various sets of target states and heralding measurements, then compare them with those of the single-photon-source model of a similar mode scale, in order to verify the computational feasibility of our model.

We encode the Bell state (Fig. 3) in two dual-rail qubits across four physical modes. The heralding modes are set to all-click or only one mode vacuum, depending on whether the photon number from squeezing is even

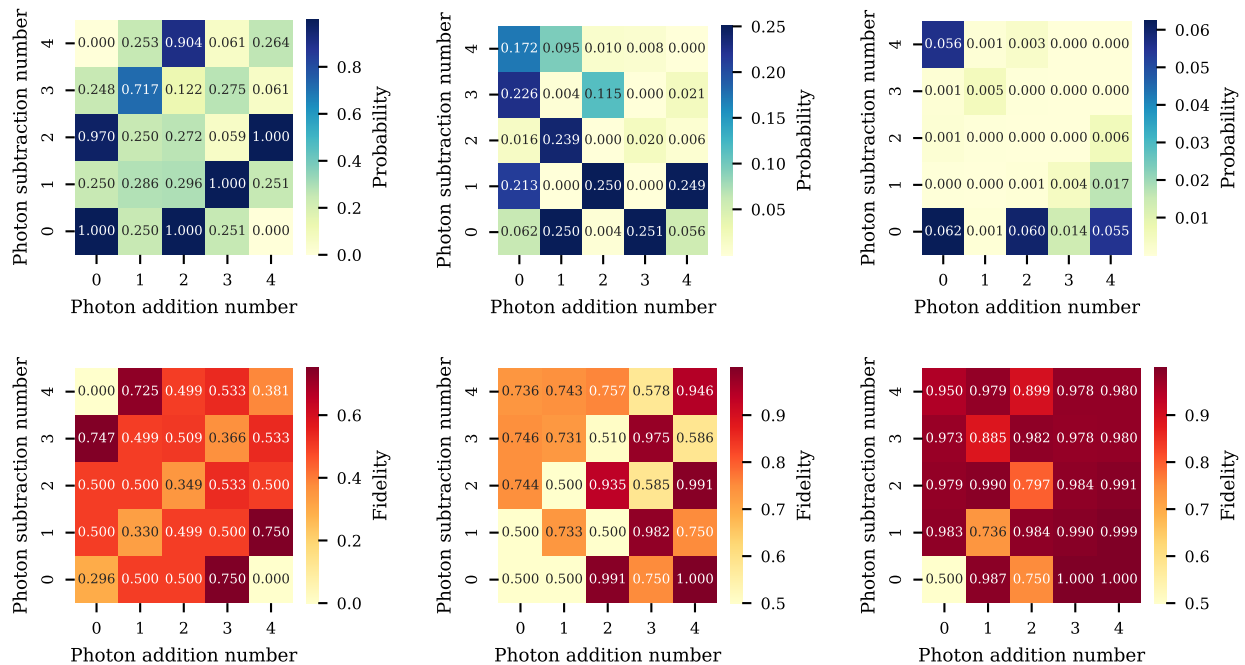


FIG. 5. Probabilities (top row) and fidelities (bottom row) of the Bell state generated as a function of photon addition and subtraction for different numbers of heralding modes as 1, 2 and 3 in each column.

or not. We set the number of heralding modes to two for comparison with a single-photon input model of the same scale, both of which converge within 10^2 iterations. When extended to the generation of GHZ (Fig. 4) encoded in three dual-rail qubits across six physical modes, we set the number of heralding modes to four to match the single-photon input model of comparable scale, which also achieves convergence within 10^2 iterations. This indicates that our Gaussian-source model exhibits comparable optimization complexity to the single-photon-source model in various heralded entanglement generation tasks, while achieving the stable optimal probability and fidelity. Compared with the Bell and GHZ states, some superposition terms of the W state share identical photon occupations on certain physical modes. This partial mode overlap makes the optimization of the probability and fidelity more difficult to converge and more susceptible to local optima.

B. Photon Addition and Subtraction

In the single-photon-source model, the number of input photons and heralding modes constrains the probability and fidelity of heralded entanglement generation [39], which remains equally important in our model. Since Gaussian states do not conserve photon number, single-photon conditional measurements cannot completely eliminate the limitations imposed by vacuum and multi-photon components on the output state fidelity. Introducing additional non-Gaussian operations, such as

photon addition and subtraction, can help enhance the performance of entanglement generation. Therefore, selecting the optimal heralding modes and photon addition/subtraction configurations is a key research direction for achieving efficient and high-fidelity entangled state generation.

We plot heatmaps of the heralded generation probability and fidelity for Bell states under different configurations as Fig. 5. Compared with their positive impact on enhancing the non-classicality of Gaussian states and on the heralded generation of cat and Gottesman–Kitaev–Preskill (GKP) states [27], photon addition and subtraction exhibit a more variable influence on the heralded generation of dual-rail encoded entangled states. In certain configurations, such as adding two photons and subtracting none with 2 heralding modes, the Gaussian-state parameters can be optimized to achieve an acceptable probability of generating entangled states with high fidelity. In the best configuration, a Bell state with a fidelity of 0.991 can be generated with a probability of 0.004. Considering the probabilistic heralded single-photon sources, their efficiency is comparable to that of the single-photon source model. In other configurations, however, the optimization tends to become trapped in local optima or fails to improve the generation performance that simultaneously balance the probability and fidelity.

The results show that increasing the number of heralding modes tends to reduce the generation probability while improving the fidelity, whereas increasing the number of photon additions and subtractions generally en-

hances both the probability and fidelity. Moreover, photon addition proves to be more effective than photon subtraction, as it more effectively suppresses the contributions of the vacuum and multi-photon components more in the output state. When the number of photon addition reaches four and the number of heralding modes exceeds 2, the fidelity converges to 1, at which point the Gaussian-source model becomes essentially equivalent to the single-photon-source model with Gaussian noise.

In the models for the generation of GHZ states, the additional heralding modes and photon additions/subtractions increase the number of modes, leading to an exponential growth in the computational complexity of the Hafnian. Here, we present the optimization results only for 4 heralding modes in Fig. 6.

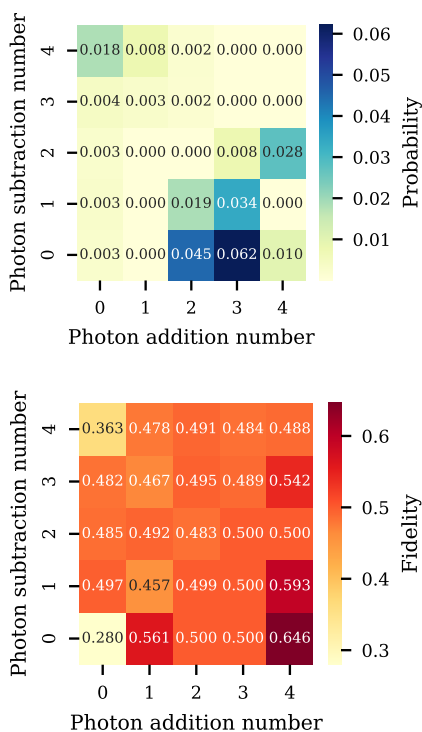


FIG. 6. Probability and fidelity of the GHZ state generated as a function of photon addition and subtraction for the numbers of heralding modes as 4.

The results show that increasing the number of photon additions and subtractions can enhance the probability and fidelity in certain configurations. In other configurations such as adding 1 photon with subtracting 1 the optimization tends to the lower probability and fidelity. The computational complexity of each optimization iteration increases exponentially with the number of modes in the system, and the total parameter space grows accordingly. This makes it very challenging to directly obtain high-probability, high-fidelity GHZ states through optimization.

C. Post-selecting Non-vacuum States

In the heralded state-generation model considered here, a residual vacuum component in the output modes is unavoidable. This vacuum contribution originates from the intrinsic vacuum dominance of low-gain Gaussian sources and cannot be completely eliminated by a finite number of heralding measurements or photon addition/subtraction operations. As a result, even when the heralding conditions are satisfied, the vacuum component inevitably degrades the fidelity of the generated target states.

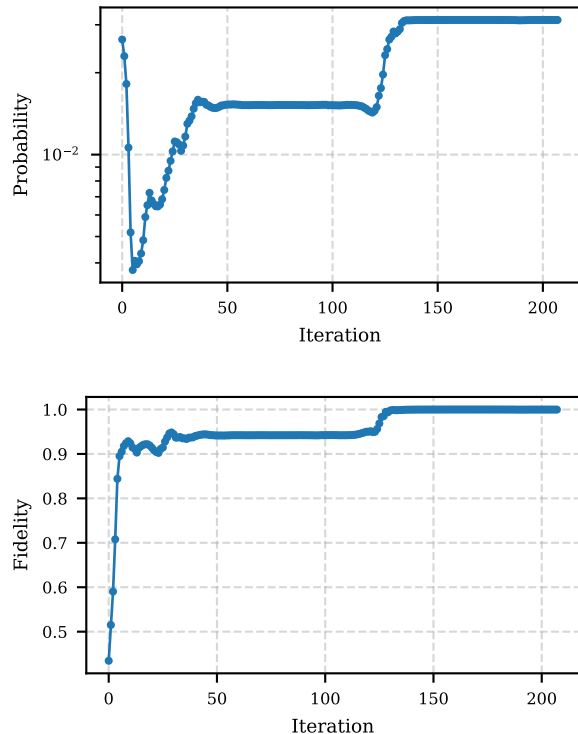


FIG. 7. Probability and fidelity of the Bell state generated with post-selecting non-vacuum states as a function of optimal steps. The weights w_1 , w_2 and ϵ are set to 10, 1 and 10^{-4} .

To mitigate this effect, we adopt a post-selection strategy that removes vacuum contributions at the level of the encoded output state. Following Ref. [30], we assume an ideal on-off quantum nondemolition (QND) measurement applied to the output modes, which discriminates vacuum from non-vacuum events without disturbing the encoded dual-rail subspace. If the purpose is solely to verify the generated state, the QND measurement may be replaced by standard threshold detectors in a practical implementation, which are readily available experimentally. We post-select only those events in which each pair of physical modes encoding a dual-rail qubit contains at least one photon. Importantly, this procedure does not modify the state-preparation process itself, nor does it introduce additional heralding modes or photon addi-

tion/subtraction operations; instead, it operationally restricts the measurement outcomes to the logical subspace of interest.

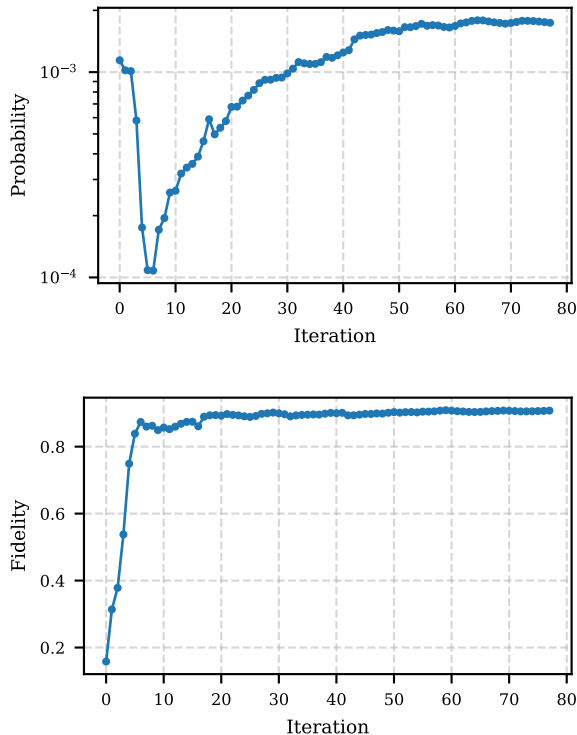


FIG. 8. Probability and fidelity of the GHZ state generated with post-selecting non-vacuum states as a function of optimal steps. The weights w_1 , w_2 and ϵ are set to 10, 1 and 10^{-4} .

In this context, it is useful to distinguish between the raw heralding success probability and the effective probability after post-selection. The probability reported throughout this subsection corresponds to the experimentally observable effective success probability, which includes both the heralding probability and the additional non-vacuum post-selection filtering. While the latter inevitably reduces the total event rate, it leads to a substantial suppression of vacuum-induced errors and thus significantly enhances the fidelity of the generated states.

Fig. 7 shows the evolution of the optimized probability and fidelity for a Bell-state target under non-vacuum post-selection. The optimization weights are chosen as $w_1 = 10$, $w_2 = 1$, and $\epsilon = 10^{-4}$, which prioritize the suppression of vacuum contributions during the early stages of the optimization. We have verified that the qualitative improvement is robust against moderate variations of these parameters.

For the Bell-state target, we obtain an optimal effective success probability of 0.0312 and a fidelity of 0.9998, using only two heralding modes and without photon addition or subtraction. Given the low-gain limitation inherent to probabilistic single-photon sources,

this performance is more efficient than that of single-photon-source-based schemes with a comparable number of resources [21]. In particular, increasing the number of heralding modes typically leads to an order-of-magnitude reduction in success probability, whereas the present post-selection strategy achieves a high fidelity with only a modest additional filtering cost.

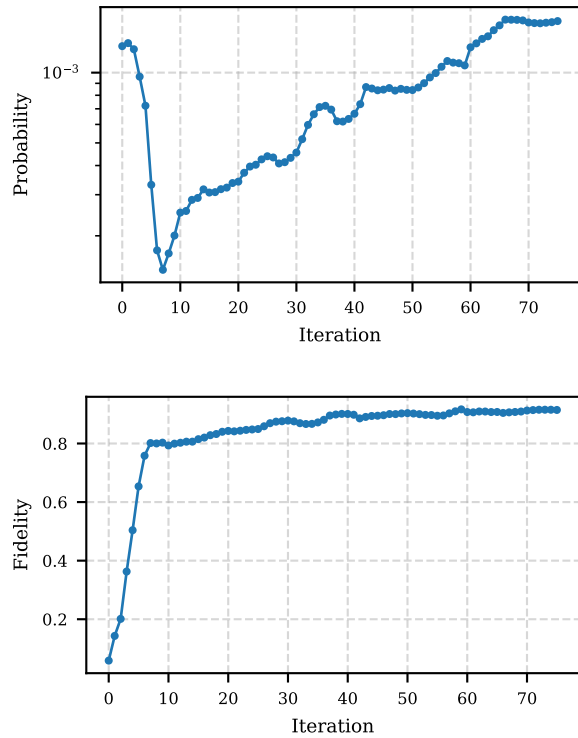


FIG. 9. Probability and fidelity of the W state generated with post-selecting non-vacuum states as a function of optimal steps. The weights w_1 , w_2 and ϵ are set to 10, 1 and 10^{-4} .

We further apply the same post-selection procedure to models targeting multipartite entangled states. For the GHZ and W states in Fig. 8 and Fig. 9, we obtain optimal effective success probabilities of 0.00174 and 0.00166, with corresponding fidelities of 0.9075 and 0.9145, respectively. The reduced fidelities compared to the Bell-state case can be attributed to the increased sensitivity of multipartite entanglement to residual vacuum components and mode correlations. Notably, this approach preserves the same number of heralding modes and Gaussian sources as those employed in single-photon-source-based schemes for GHZ-state generation [22], while achieving competitive performance without relying on deterministic single-photon inputs.

As shown in the preceding sections, photon addition provides an effective means to improve the fidelity of multipartite entangled states in models without vacuum post-selection. The same strategy can be directly applied in the present post-selected setting. In particular, we find that introducing photon addition during the state-

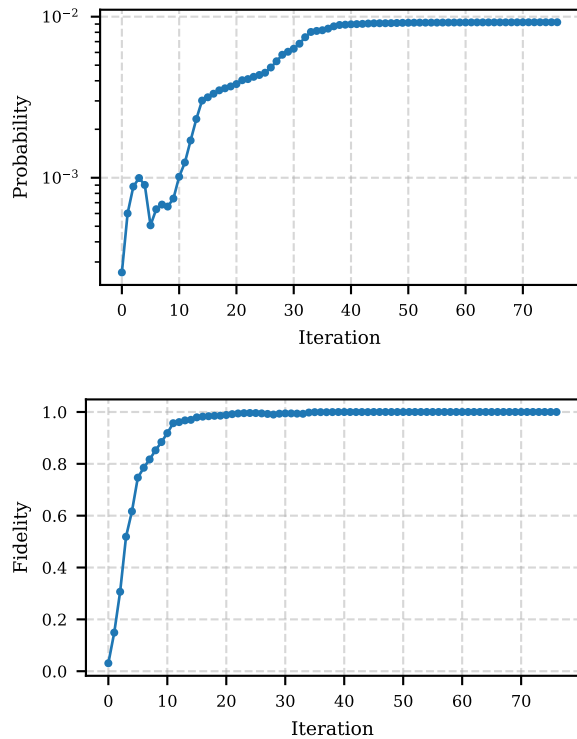


FIG. 10. Probability and fidelity of the GHZ state generated with post-selecting non-vacuum states and 2 photons added as a function of optimal steps. The weights w_1 , w_2 and ϵ are set to 10, 1 and 10^{-4} .

preparation stage remains effective in suppressing residual non-ideal components that are not fully removed by the non-vacuum post-selection alone.

For both GHZ and W state targets, we observe that adding two photons is already sufficient to raise the optimized effective fidelity to values very close to unity. Increasing the number of added photons beyond this point yields only marginal improvement and is therefore not considered. The corresponding optimization trajectories of the effective fidelity and success probability are shown in Fig. 10 and Fig. 11, where the same non-vacuum post-selection criterion is applied.

These results demonstrate that the combination of non-vacuum post-selection and a minimal amount of photon addition enables the high-fidelity generation of multipartite entangled states without increasing the number of heralding modes.

D. Robustness

Due to experimental constraints, the parameters of Gaussian states cannot usually be perfectly adjusted to match the optimized values and are subject to fluctuations over long time scales. This necessitates that the model maintain high entanglement generation probabil-

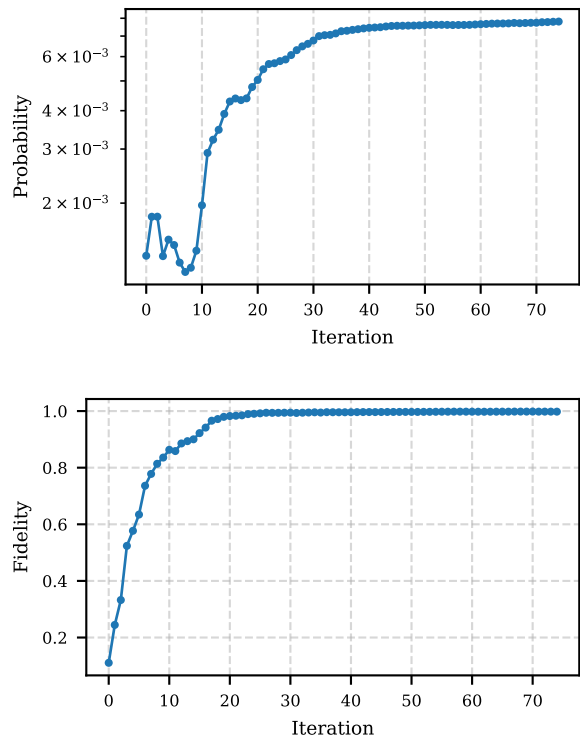


FIG. 11. Probability and fidelity of the W state generated with post-selecting non-vacuum states and 2 photons added as a function of optimal steps. The weights w_1 , w_2 and ϵ are set to 10, 1 and 10^{-4} .

ity and fidelity under a certain level of perturbation.

We assess the robustness of the heralded generation by examining how the probability and fidelity vary with changes in the Gaussian state parameters, which is crucial for its experimental implementation, as it ensures stable performance under parameter fluctuations. We introduce random perturbations to each parameter and calculate the differences in the entanglement generation probability and fidelity between the perturbed and optimized results. The results in Fig. 12 show that the variations in probability and fidelity follow the same trend as the parameter perturbations: when each parameter fluctuation is below 1%, the corresponding changes in probability and fidelity remain within 0.5% and 3%. This model exhibits good robustness against small perturbations, with the generation probability being more stable than the fidelity.

V. DISCUSSION

In this work, we have optimized a Gaussian-source-based heralded entanglement generation model and presented the optimal generation probabilities and fidelities for dual-rail encoded Bell, GHZ, and W states at the same scale as the single-photon input model. Ow-

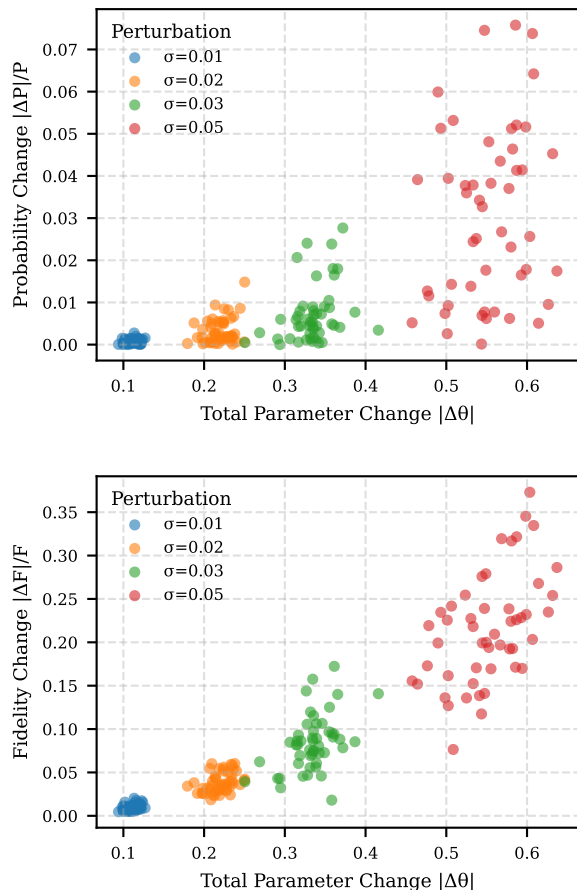


FIG. 12. Variations in probability and fidelity as functions of the total parameter change under random perturbations. Different colors indicate the maximum variation applied to each parameter in the random perturbations.

ing to the inherent vacuum and multiphoton components in Gaussian states, the Gaussian-input scheme exhibits no intrinsic advantage over single-photon inputs, and its performance further degrades in higher-dimensional or multipartite settings. By adjusting the heralding modes and incorporating photon addition and subtraction, how-

ever, the optimal probabilities and fidelities can be significantly improved. Through optimization under various conditions, we identified Gaussian-state configurations achieving higher fidelity and generation probability. The introduced non-Gaussian operations further enhance the non-classicality of the output state and improve the efficiency of heralded entanglement generation, consistent with observations reported in other Gaussian-based heralded state generation studies. To further suppress the influence of vacuum and multiphoton components, photon-number-resolving or quantum nondemolition measurements could be applied for post-selection of the desired entangled state, which effectively enhances the output fidelity under low-gain conditions. Post-selecting on the modes associated with each qubit leads to a pronounced improvement in the fidelity. In this regime, the generation probability of the entangled state exhibits a clear advantage over heralded generation schemes based on probabilistic single-photon sources.

To bridge the gap between theoretical models and experimental implementations, we analyzed the robustness of the generation performance under parameter perturbations of the Gaussian sources. The results indicate that when the fluctuations in model parameters are below 1%, the resulting variations in probability and fidelity remain within 3%, demonstrating strong resilience against experimental imperfections.

With the rapid development of Gaussian light sources and integrated photonics, this framework can be readily adapted to realistic experimental platforms. Future work may combine the present optimization approach with specific device parameters to design resource-efficient and experimentally feasible entanglement generation schemes across a variety of photonic architectures.

ACKNOWLEDGMENTS

This work was supported by Quantum Science and Technology-National Science and Technology Major Project (No. 2021ZD0301200), National Natural Science Foundation of China (Nos. 12474494, 12204468).

-
- [1] R. Horodecki, P. Horodecki, M. Horodecki, and K. Horodecki, *Rev. Mod. Phys.* **81**, 865 (2009).
 - [2] M. A. Nielsen and I. L. Chuang, *Quantum Computation and Quantum Information: 10th Anniversary Edition* (Cambridge University Press, 2010).
 - [3] N. Brunner, D. Cavalcanti, S. Pironio, V. Scarani, and S. Wehner, *Rev. Mod. Phys.* **86**, 419 (2014).
 - [4] A. K. Ekert, *Phys. Rev. Lett.* **67**, 661 (1991).
 - [5] C. H. Bennett, G. Brassard, C. Crépeau, R. Jozsa, A. Peres, and W. K. Wootters, *Phys. Rev. Lett.* **70**, 1895 (1993).
 - [6] R. Raussendorf and H. J. Briegel, *Phys. Rev. Lett.* **86**, 5188 (2001).
 - [7] V. Giovannetti, S. Lloyd, and L. Maccone, *Science* **306**, 1330 (2004).
 - [8] M. Erhard, M. Krenn, and A. Zeilinger, *Nature Reviews Physics* **2**, 365 (2020).
 - [9] N. Friis, O. Marty, C. Maier, C. Hempel, M. Holzäpfel, P. Jurcevic, M. B. Plenio, M. Huber, C. Roos, R. Blatt, and B. Lanyon, *Phys. Rev. X* **8**, 021012 (2018).
 - [10] J.-W. Pan, Z.-B. Chen, C.-Y. Lu, H. Weinfurter, A. Zeilinger, and M. Żukowski, *Rev. Mod. Phys.* **84**, 777 (2012).
 - [11] C. Weedbrook, S. Pirandola, R. García-Patrón, N. J. Cerf, T. C. Ralph, J. H. Shapiro, and S. Lloyd, *Rev. Mod. Phys.* **84**, 621 (2012).

- [12] G. Adesso, S. Ragy, and A. R. Lee, *Open Systems & Information Dynamics* **21**, 1440001 (2014).
- [13] A. Mari and J. Eisert, *Phys. Rev. Lett.* **109**, 230503 (2012).
- [14] R. Takagi and Q. Zhuang, *Phys. Rev. A* **97**, 062337 (2018).
- [15] M. G. Genoni and M. G. A. Paris, *Phys. Rev. A* **82**, 052341 (2010).
- [16] D. Su, C. R. Myers, and K. K. Sabapathy, *Phys. Rev. A* **100**, 052301 (2019).
- [17] M. Dakna, J. Clausen, L. Knöll, and D.-G. Welsch, *Phys. Rev. A* **59**, 1658 (1999).
- [18] A. Ourjoumtsev, R. Tualle-Brouri, J. Laurat, and P. Grangier, *Science* **312**, 83 (2006).
- [19] J. Fiurášek, *Phys. Rev. A* **80**, 053822 (2009).
- [20] C. Navarrete-Benlloch, R. García-Patrón, J. H. Shapiro, and N. J. Cerf, *Phys. Rev. A* **86**, 012328 (2012).
- [21] S. A. Fldzhyan, M. Y. Saygin, and S. P. Kulik, *Phys. Rev. Res.* **3**, 043031 (2021).
- [22] F. V. Gubarev, I. V. Dyakonov, M. Y. Saygin, G. I. Struchalin, S. S. Straupe, and S. P. Kulik, *Phys. Rev. A* **102**, 012604 (2020).
- [23] S. Chen, L.-C. Peng, Y.-P. Guo, X.-M. Gu, X. Ding, R.-Z. Liu, J.-Y. Zhao, X. You, J. Qin, Y.-F. Wang, Y.-M. He, J. J. Renema, Y.-H. Huo, H. Wang, C.-Y. Lu, and J.-W. Pan, *Phys. Rev. Lett.* **132**, 130603 (2024).
- [24] H. Cao, L. M. Hansen, F. Giorgino, L. Carosini, P. Zahálka, F. Zilk, J. C. Loredó, and P. Walther, *Phys. Rev. Lett.* **132**, 130604 (2024).
- [25] P. Caspar, E. Verbanis, E. Oudot, N. Maring, F. Samara, M. Caloz, M. Perrenoud, P. Sekatski, A. Martin, N. Sangouard, H. Zbinden, and R. T. Thew, *Phys. Rev. Lett.* **125**, 110506 (2020).
- [26] M. V. Larsen, X. Guo, C. R. Breum, J. S. Neergaard-Nielsen, and U. L. Andersen, *Science* **366**, 369 (2019).
- [27] V. Crescimanna, A. Z. Goldberg, and K. Heshami, *Phys. Rev. A* **109**, 023717 (2024).
- [28] D. Sychev, A. Ulanov, and A. e. a. Pushkina, *Nature Photonics* **11**, 379 (2017).
- [29] C. N. Gagatsos and S. Guha, *Phys. Rev. A* **99**, 053816 (2019).
- [30] P. Dhara, S. J. Johnson, C. N. Gagatsos, P. G. Kwiat, and S. Guha, *Phys. Rev. Appl.* **17**, 034071 (2022).
- [31] J. Arrazola, V. Bergholm, and K. Brádler, *Nature* **591**, 54 (2021).
- [32] S. Shekhar, W. Bogaerts, L. Chrostowski, J. E. Bowers, M. Hochberg, R. Soref, and B. J. Shastri, *Nature Communications* **15**, 751 (2024).
- [33] C. S. Hamilton, R. Kruse, L. Sansoni, S. Barkhofen, C. Silberhorn, and I. Jex, *Phys. Rev. Lett.* **119**, 170501 (2017).
- [34] J. F. Clauser, M. A. Horne, A. Shimony, and R. A. Holt, *Phys. Rev. Lett.* **23**, 880 (1969).
- [35] M. Walschaers, *PRX Quantum* **2**, 030204 (2021).
- [36] R. Kruse, C. S. Hamilton, L. Sansoni, S. Barkhofen, C. Silberhorn, and I. Jex, *Phys. Rev. A* **100**, 032326 (2019).
- [37] B. Gupt, J. Izaac, and N. Quesada, *Journal of Open Source Software* **4**, 1705 (2019).
- [38] W. R. Clements, P. C. Humphreys, B. J. Metcalf, W. S. Kolthammer, and I. A. Walmsley, *Optica* **3**, 1460 (2016).
- [39] S. Stanisic, N. Linden, A. Montanaro, and P. S. Turner, *Phys. Rev. A* **96**, 043861 (2017).